

# Ultra-Large Silicon Diode for Characterizing Low-Intensity Radiation Environments

Kacper Bilko<sup>1</sup>, Graduate Student Member, IEEE, Rubén García Alía<sup>2</sup>, Member, IEEE, Sylvain Girard<sup>3</sup>, Senior Member, IEEE, Mario Sacristan Barbero<sup>4</sup>, Member, IEEE, Matteo Cecchetto<sup>5</sup>, Camille Belanger-Champagne<sup>6</sup>, Member, IEEE, Matteo Brucoli<sup>7</sup>, Salvatore Danzeca<sup>8</sup>, Alex Hands<sup>9</sup>, Pedro Martín Holgado<sup>10</sup>, Student Member, IEEE, Yolanda Morilla Garcia<sup>11</sup>, Amor Romero Maestre<sup>12</sup>, Marc Sebban<sup>13</sup>, and Markus Widorski<sup>14</sup>

**Abstract**—We present applications of a large commercial silicon diode (50 cm<sup>2</sup> × 500 μm) for monitoring low-intensity radiation fields, together with benchmarks via Monte Carlo simulations. After energy calibration with monoenergetic proton and alpha beams in the 2–8-MeV range, we show that the detector is capable of measuring atmospheric radiation at the ground level, not only in terms of a total number of events but also through their energy deposition distribution. Focusing on the atmospheric-like neutron spectrum, we prove that the diode detection cross section is more than five orders of magnitude larger with respect to static random access memory (SRAM)-based solutions and highlight the potential use cases in the accelerator’s radiation environment.

**Index Terms**—Atmospheric neutrons, CERN, centro nacional de aceleradores (CNA), detector, diode, FLUKA, Geant4, silicon, TRIUMF.

## I. INTRODUCTION

RADIATION environment monitoring is a fundamental ingredient in the more global radiation hardness assurance (RHA) strategy for CERN accelerators [1], [2], both in terms of defining the tolerance of radiation systems to be installed in the accelerator in the future and applying efficient mitigation measures for radiation effects negatively impacting the operation and performance of different accelerator systems. Such a monitoring approach is fulfilled mainly through the

RadMON system [3], [4], consisting of static random access memories (SRAMs) to measure the thermal and high-energy hadron fluences, and complemented through FLUKA radiation-level simulations [5], [6], [7]. It was a key to successful mitigation measures in the large Hadron Collider (LHC) during Run 1 (2010–2012), Long Shutdown 1 (LS1) (2013–2014) [8], the beginning of Run 2 (2015), and more recently (2021) in the super proton synchrotron (SPS) accelerator [9].

In the case of the LHC [10], the RadMON provides a very performant and cost-efficient solution to monitor radiation levels in the tunnel and nearby shielded alcoves, mainly around interaction points (IPs) 1, 5 (high-luminosity experiments), and 7 (collimation), concentrating a very large fraction of the system units causing radiation effects issues in the accelerator, and subject to annual radiation levels in the order of a few 10<sup>8</sup> HEH/cm<sup>2</sup>/year (high-energy Hadrons) [1]. Indeed, the calibrated SRAM sensing elements, along with the radiation tolerant readout electronics, offer a solution with a sensitivity that can be estimated based on the typical SRAM bit SEU cross section ( $\sim 10^{-14}$  cm<sup>2</sup>/bit) for high-energy protons (or, more generally hadrons, including also neutrons and protons) and a number of bits per SRAM, or group of SRAMs ( $\sim 10$  Mb) yielding a total cross section of  $\sim 10^{-6}$  cm<sup>2</sup>/device, and therefore recording a statistically meaningful amount of events (a few tens) for one year of operation with the radiation level introduced above. However, after successful LHC radiation effects’ mitigation measures introduced during Run 1 and LS1 (2013–2014) mainly based on shielding, relocation, and system patches, as well as the prevention measures associated with the development, qualification, and deployment of radiation-tolerant systems during Run 2 (2015–2018) and LS2 (2019–2021), the relative contribution to the LHC critical single-event effect (SEE) rate from commercial modules and systems installed in areas with significantly lower radiation levels has increased. In fact, based on the past experience, an area at CERN is only declared as radiation-safe for electronics for critical systems if its radiation levels, in terms of HEH fluxes (note: we do not cover thermal neutron levels and related electronics sensitivity in this work), are below  $3 \cdot 10^6$  HEH/cm<sup>2</sup>/year, i.e., roughly a factor 30 above the sea-level neutron background. This value is based on a combination of the acceptable functional SEE

Manuscript received 16 October 2023; revised 16 November 2023; accepted 27 November 2023. Date of publication 30 November 2023; date of current version 18 April 2024. This work (TRIUMF beamtime) was supported in part by the European Union’s Horizon 2020 Research and Innovation Program under Grant 101008126. (Corresponding author: Kacper Bilko.)

Kacper Bilko is with the CERN, 1211 Geneva, Switzerland, and also with the Université Jean Monnet, 42100 Saint-Étienne, France (e-mail: kacper.bilko@cern.ch).

Rubén García Alía, Mario Sacristan Barbero, Matteo Cecchetto, Matteo Brucoli, Salvatore Danzeca, and Markus Widorski are with the CERN, 1211 Geneva, Switzerland.

Sylvain Girard is with the Université Jean Monnet, 42100 Saint-Étienne, France, and also with the Institut Universitaire de France (IUF), Ministère de l’Enseignement Supérieur et de la Recherche, 75005 Paris, France.

Camille Belanger-Champagne and Alex Hands are with the TRIUMF, Vancouver, BC V6T 2A3, Canada.

Pedro Martín Holgado, Yolanda Morilla Garcia, and Amor Romero Maestre are with the CNA, 41092 Seville, Spain.

Marc Sebban is with the Université Jean Monnet, 42100 Saint-Étienne, France.

Color versions of one or more figures in this article are available at <https://doi.org/10.1109/TNS.2023.3337839>.

Digital Object Identifier 10.1109/TNS.2023.3337839

TABLE I  
CHARACTERISTICS OF THE USED SILICON DETECTOR

Ref.	Applied bias (V)	Model	Thickness (mm)	Exposed Si surface (cm <sup>2</sup> )
1	130 (170)	PD 5000-75-500AM	0.5	50

rate for critical accelerator systems, a typical number of units per critical distributed system, and the distribution and upper limit of commercial system-level SEE cross sections, based on CERN's experience in both qualification and operation conditions.

Therefore, accurately monitoring locations with such levels based on the RadMON SRAM sensors introduced above is challenging, especially when statistically meaningful results are needed in time frames potentially much shorter than one full operational year. This is the case in the LHC arc sectors [11], some shielded alcoves [12], or beyond accelerator applications, e.g., during avionic or stratospheric measurements [13].

Hence, in this work, we introduce the calibration and application of a significantly more sensitive radiation monitor, operated with the current-sensitive preamplifier [14], capable of accurately measuring HEH levels in the order of those obtained from cosmic-ray-induced neutrons at sea level. The setup provides not only a count rate but also additional information on the energy deposition distribution in silicon of the associated environment, which is essential for the Monte Carlo simulation benchmarks.

This article is structured as follows: in Section II, both the detector and experimental setup are described, Section III presents the energy calibration of the detector against monoenergetic beams and dose-rate calibration under Co-60 exposition. Section IV demonstrates the use of the detector for the monitoring of low-intensity environments, both through the measurements and Monte Carlo simulations. Section V features the conclusions and outlook of the work.

## II. EXPERIMENTAL SETUP

The detector is a silicon diode, as depicted in Fig. 1, operated under the reverse bias. Its main characteristics are tabulated in Table I. A 110-V bias voltage, according to the manufacturer certificate, is required for a full depletion. The detector was operated at all times at 130 V (recommended bias), with a single run at 170 V (maximum allowed bias). Higher bias voltage accelerates the charge collection process, leading to larger signal amplitudes, and therefore allows for a slight improvement of the detection limit, as the threshold is on the amplitude value. The detector features a very thin (below 50 nm) dead layer.

The detector is biased through the CIVIDEC C2-HV broadband current-sensitive preamplifier (certified amplification of  $g = 43.9$  dB). The signal is acquired and digitized via CAEN DT5751 1 GS/s (10-bit resolution). The outcome of each energy deposition event is a voltage signal ( $I(t) = V(t)/R$ ,  $R = 50 \Omega$ ), acquired with 1-ns resolution. An example of

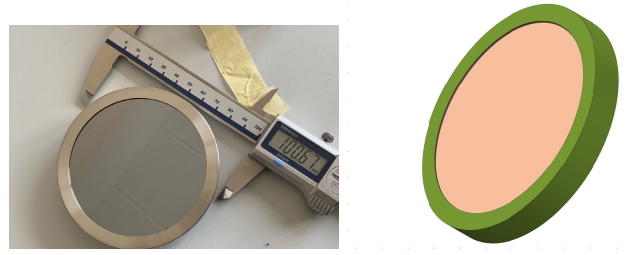


Fig. 1. Silicon solid-state PIPS detector (Mirion PD 5000-75-500AM) with the corresponding model used in the FLUKA Monte Carlo simulations.

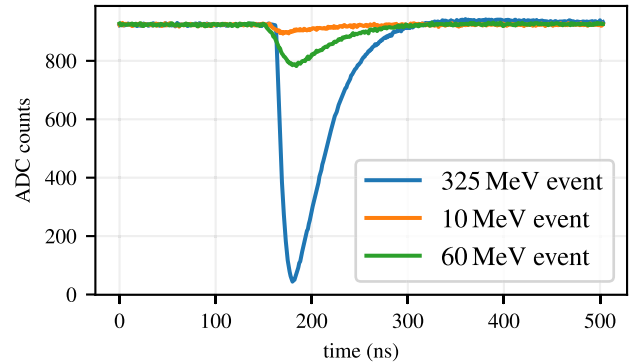


Fig. 2. Examples of the registered single energy deposition events, registered during the exposure to the atmospheric radiation, described in Section IV-B.

such an event is depicted in Fig. 2. In the postprocessing, the retrieved current signal (with the baseline subtracted) is integrated to retrieve the number of generated  $e$ -hole pairs ( $Q/e$ , where  $Q$  is the deposited charge and  $e$  is the elementary charge). The related deposited energy  $E_{\text{dep}}$  is calculated according to (1) where  $k$  is a correction factor, obtained through the calibration described in Section III, and  $E_h \approx 3.6$  eV is the energy needed to create electron-hole pair in silicon [15]

$$E_{\text{dep}} = k \cdot E_h \frac{Q}{e} = k \frac{E_h}{ge} \int I(t) dt. \quad (1)$$

## III. DETECTOR CALIBRATION

### A. Energy Calibration at CNA

To retrieve the  $k$  factor [See (1)], allowing to calculate deposited energy from the detector's signal, a calibration campaign was performed in Centro Nacional de Aceleradores (CNA; Seville, ES) [16], [17].

The irradiations were carried out in vacuum ( $\sim 10^{-7}$  mbar) using proton and alpha particles accelerated by a 3-MV Tandem accelerator and depositing its entire energy in the silicon volume. Complementarily, the tests included a triple-alpha ( $^{239}\text{Pu}$ ,  $^{241}\text{Am}$ ,  $^{244}\text{Cm}$ ) source calibration, as depicted in Fig. 3. However, given the energy resolution of the setup, it is not possible to disentangle each of the alpha energies in the measured deposition spectrum. According to the manufacturer specification, the energy resolution of the detector itself, in terms of full width half maximum (FWHM), is equal to 67 keV for alpha particles of 5486 keV. The FWHM is factor 10 lower than the measured value. One of the reasons could be: 1) collimation of the alpha beam by the manufacturer

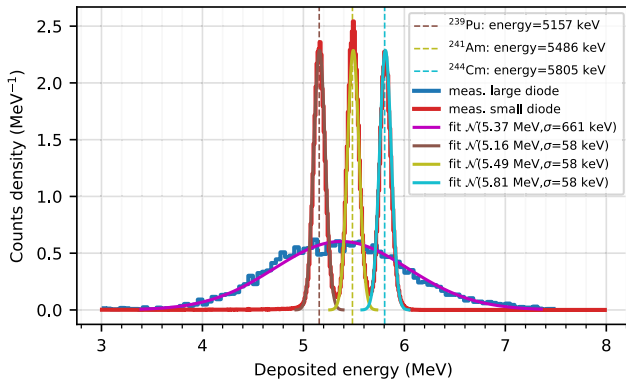


Fig. 3. Measured energy deposition distribution with triple-alpha ( $^{239}\text{Pu}$ ,  $^{241}\text{Am}$ ,  $^{244}\text{Cm}$ ) source as measured by the detector (*large diode*) listed in Table 1. The energy resolution of the detector (with the current-sensitive preamplifier and described readout chain) is worse when compared with *small diode* ( $0.5\text{ cm}^2 \times 300\text{ }\mu\text{m}$ ).

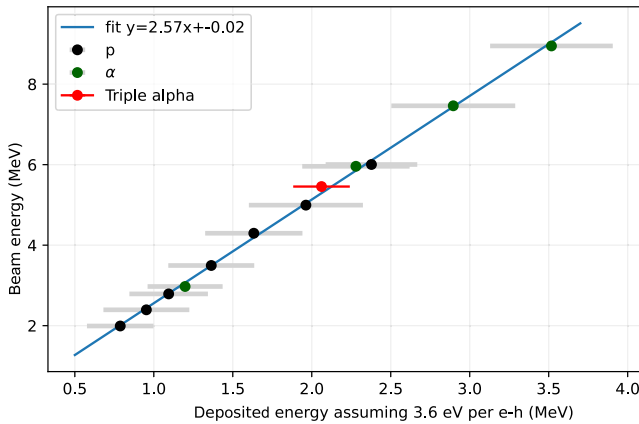


Fig. 4. Energy calibration of the silicon solid-state detector. The plot depicts the beam energy (that is equal to the real deposited energy) as a function of the measured deposited energy, assuming on average  $3.6\text{ eV}$  per e-h pair [ $k = 1$  in (1)], with the fit linear model. The slope of the fit ( $k = 2.57$ ) corresponds to the correction factor for the experimental setup, according to (1). The  $x$ -error bars correspond to  $\sigma$  of the Gaussian function retrieved while fitting to the measured energy and therefore indicate the energy resolution of the detector.

and 2) use a different readout chain, in particular a charge-sensitive amplifier. The latter could improve the resolution significantly at the cost of a worse time resolution. In the targeted radiation environments (accelerators), a very good time resolution is essential to discard false pulses, resembling particle interactions, which are induced by high-frequency noise, e.g., due to magnet operation.

The beam (or source) energy was equal to the total deposited energy, as the tests were performed in a vacuum and the particle range was significantly below the active silicon thickness. The beam energies, entirely deposited in silicon, as a function of calculated deposited energies, assuming  $k = 1$  and the certified preamplifier gain, are presented in Fig. 4. All the measurements are highly collinear and the related slope  $k = 2.57$  is the correction factor that needs to be applied in (1) to retrieve energy deposition in silicon.

In addition to the triple-alpha source, the irradiations were performed with the monoenergetic beams and the related energy resolution is primarily due to the detector's response.

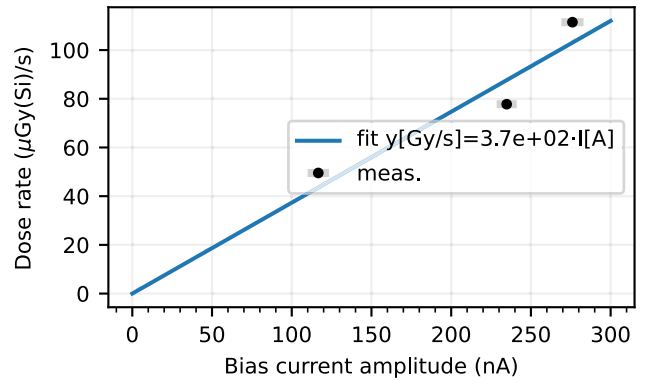


Fig. 5. Dose-rate calibration of the silicon solid-state detector in a Co-60 facility, with the fit linear model. The  $x$ -axis corresponds to the leakage current measured at the output of the preamplifier and  $y$ -axis to the dose rate measured by the PTW 30010 Farmer ionization chamber.

The beam was collimated with a polyethylene layer to decrease the instantaneous count rate, which could introduce some energy straggling, and therefore further increase the spread in the measured deposited energy. This, however, does not impact the calibration factor  $k$ .

#### B. Dose-Rate Calibration With Co-60 at CNA

The gamma-radiation laboratory at CNA is based on a Co-60 irradiator [17]. Two associated gamma rays with energies of 1.17 and 1.33 MeV are emitted, providing different square irradiation fields. The dosimetry system consists of a PTW 30010 Farmer ionization chamber (volume  $0.6\text{ cm}^3$ ).

The diode setup allows measuring a change in the bias current that is related to the power (dose rate) that is being deposited in the detector. As opposed to the previous paragraph, the deposited energy is not calculated event-by-event, but rather as a time integral of the dose rate, retrieved through the leakage current change. The reference dose rate was measured by the ionization chamber provided by the facility, and the corresponding change in the measured bias current is depicted in Fig. 5.

However, this current-based measurement mode, due to power supply limitations, is representative of irradiations lasting at least 1 s and could be exploited, for example, for the dose-rate estimation during neutron irradiations.

## IV. NEUTRON SPECTRAL FIELDS: MEASUREMENTS AND SIMULATIONS

As highlighted in Section I, the targeted working environment, such as LHC-shielded alcoves, will be neutron-dominant. To demonstrate the detection capabilities in the several neutron fields, the tests were performed at: the Am-Be source, located in CALLAB at CERN [18]; at a CERN surface building under the exposure to atmospheric radiation; at the spallation neutron facility TRIUMF-BL1B [19], [20], [21]; and at the CERN accelerator environment, close to the Linear Accelerator 3 (LINAC3) [22]. The simulated energy spectra for these fields are depicted in Fig. 6 [23], [24], [25].

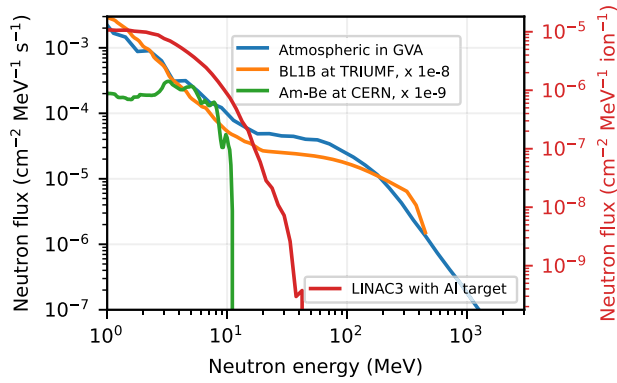


Fig. 6. Simulated neutron flux spectra for: 1) atmospheric field extracted from MAIRE tool [23], [25] for Geneva coordinates; 2) spallation neutron field at TRIUMF (BL1B); 3) Am-Be source at CERN [18]; and 4) 4.2 MeV/u  $^{16}\text{O}^{8+}$  ions impacting Al target at LINAC3 (CERN).

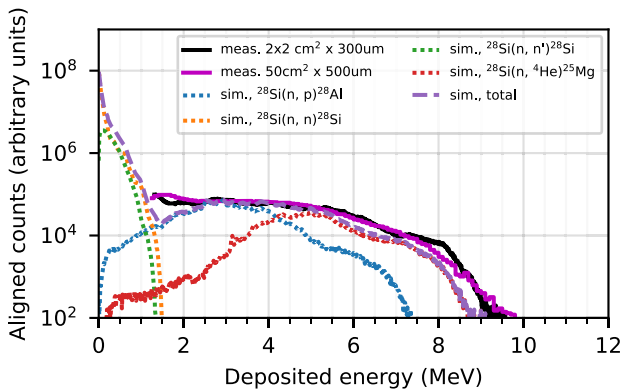


Fig. 7. Measurements of the deposited energies by the concerned detector (listed in Table I, magenta trace), and, for comparison purposes, by the smaller and thinner silicon detector (with better energy resolution, black trace). The y-normalization is arbitrary to enable the profile comparison.

### A. CERN Am-Be Neutron Source

After successful energy calibration, the first measurements in a spectral field were performed with the Am-Be neutron source [18], [26], providing neutrons with energies ranging to 11 MeV, as depicted in Fig. 6.

The measured energy deposition spectrum is presented in Fig. 7, together with Geant4 simulations retrieved via the G4SEE toolkit [27]. The simulations were further divided by the nuclear reaction channels that initiate the energy deposition process. The maximum energy that can be deposited via elastic ( $n, n'$ ) interactions is 1.5 MeV (13.3% of neutron kinetic energy). Above that energy, the energy deposition is dominated via inelastic channels, mainly ( $n, \alpha$ ) and ( $n, p$ ).

Measurements (shapes of the deposited energy spectra) are consistent with those obtained with another silicon detector, characterized by monoenergetic neutron beams [27].

### B. Atmospheric Field

The detector has been acquiring data for 55 days in an indoor location at CERN, at the ground level, as depicted in Fig. 8. The building has two floors and the experiment took place on the top one. The surface of the detector was covered with Al foils to shield the detector from visible light.

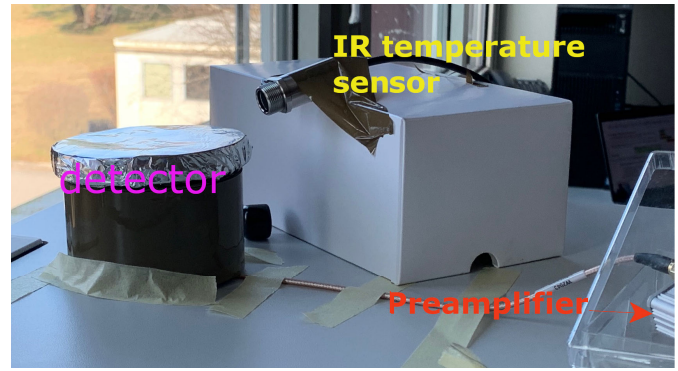


Fig. 8. Experimental setup during acquisition with the cosmic-induced radiation. Temperature measurements by the IR sensor are beyond the scope of this work.

TABLE II

STATISTICS OF REGISTERED COUNTS UNDER EXPOSURE TO: 1) GROUND-LEVEL RADIATION (ATM. GVA) AND 2) TRIUMF-BL1B SPALLATION NEUTRONS, TOGETHER WITH A NORMALIZED EVENT COUNT AND FLUKA MONTE CARLO SIMULATIONS FOR GROUND-LEVEL NEUTRON SPECTRUM. FLUX IN TRIUMF-BL1B WAS REDUCED FROM THE MAXIMUM AVAILABLE TO AVOID PILE-UPS

	Counts $E_d > 4\text{MeV}$	Counts $E_d > 10\text{MeV}$	Count rate $E_d > 10\text{MeV}$	Sim. fluence $E_k > 10\text{MeV}$	Normalised event count $E_d > 10\text{MeV}$
Atm. Geneva	0.17	1.0	$2.2 \cdot 10^{-4}$	3.0	34
TRIUMF-BL1B	25	490	$2.0 \cdot 10^3$	1400	35
Atm. sim.	2.3	91	N/A	350	26
Atm. sim. convoluted	380	95	N/A	350	27
unit	$10^5$ counts	$10^3$ counts	counts/s	$10^4\text{ cm}^{-2}$	$10^{-2}$ counts $\text{cm}^{-2}$

The measured energy deposition spectrum is depicted in Fig. 9. Over that period, 1035 energy deposition events above 10 MeV were recorded. The measurement was benchmarked against the FLUKA Monte Carlo simulations, which contained a detailed detector geometry (Fig. 1) and neutron beam with the energy spectrum retrieved through the MAIRE toolkit, accounting for the local latitude, longitude, and altitude [25]. The simulation, however, did not account for the energy resolution of the considered detector, and therefore, the simulated energy deposition spectrum was convoluted (blurring) with the Gaussian profile whose variance was approximately equal to the variance measured for a monoenergetic beam. The obtained agreement between both the curves is very good, within 25% while considering the measured versus simulated (further convoluted) event rates above 10 MeV of deposited energy, as listed in Table II.

In addition, simplified simulations of the atmospheric-neutron spectrum impacting the diode silicon volume were performed using the Geant4-based toolkit, G4SEE [27]. As opposed to FLUKA simulations, the G4SEE ones did not include the diode case due to current toolkit limitations. Profiting from a detailed scoring, we investigated which neutrons (kinetic energy) contribute to the deposited energy spectrum. Considering the region above the detection limit of the setup, energy deposition events above  $\sim 12$  MeV are driven primarily by neutrons with kinetic energies between 10 and 100 MeV.

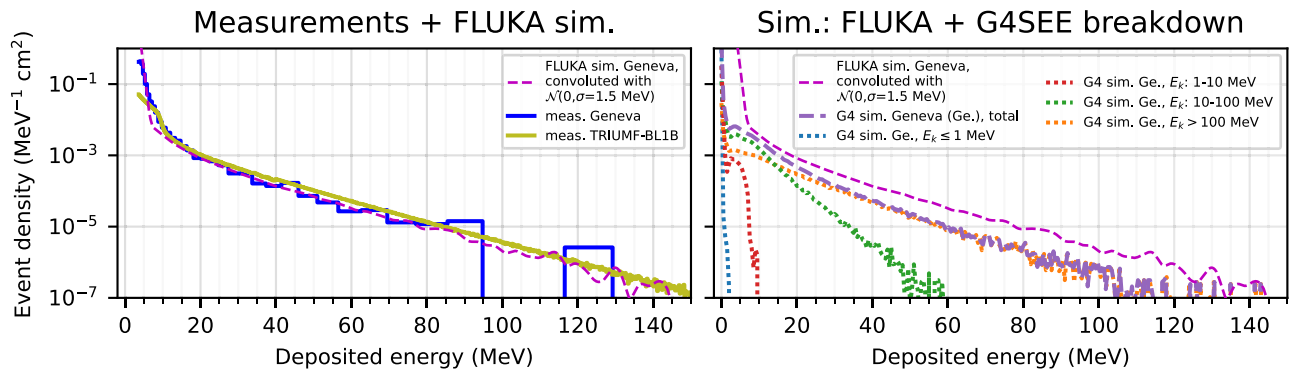


Fig. 9. Measured (on the left) and simulated (on the right) energy deposition spectra over exposure to atmospheric radiation. The FLUKA simulated energy deposition spectrum is depicted in both the subplots. The measurements were performed at CERN, over 55 days, whereas the FLUKA Monte Carlo simulations took as input the atmospheric spectrum retrieved by MAIRE and provided the energy deposited in the silicon. Also, to imitate diode energy response (low resolution), the simulated energy deposition spectrum has been convoluted with the normal distribution of  $\sigma = 1.5$  MeV. The deposited energy per a single event reached up to 325 MeV (Fig. 2).

TABLE III  
MEASURED DETECTION CROSS SECTIONS UNDER IRRADIATION  
WITH TRIUMF-BL1B NEUTRON BEAM

	Reference	Date code	Size (Mbit)	$\sigma$ (cm <sup>2</sup> )	$\frac{\sigma_{diode}}{\sigma}$
diode (bias: 130 V)	3560.317A.24.1			0.21	1.00
diode (bias: 170 V)	3560.317A.24.1			0.30	0.70
diode (small)	3705.326D.378.18			0.022	9.6
ISSI 40nm	IS61WV204816BLL-10TLI	1650	32	$6.6 \cdot 10^{-7}$	$3.2 \cdot 10^5$
Cypress 65nm	CY62167GE30-45ZXI	1731	16	$2.0 \cdot 10^{-6}$	$1.1 \cdot 10^5$
Cypress 90nm	CY62157EV30LL-45ZSXI	1843	8	$1.3 \cdot 10^{-6}$	$1.6 \cdot 10^5$
Cypress 90nm	CY62167EV30LL-45ZXA	1731	16	$6.8 \cdot 10^{-7}$	$3.1 \cdot 10^5$

### C. Neutrons From Spallation: TRIUMF-BL1B

Profiting from beamtime provided via RADNEXT [28], irradiations of the large detector at TRIUMF-BL1B were performed. The neutron beam is obtained via the 480-MeV proton beam impacting in a lead target, through spallation reactions [20]. The related neutron spectrum resembles an atmospheric one, with the cutoff due to the maximum kinetic energy of the protons (480 MeV), as depicted in Fig. 6.

The measured energy deposition spectrum is illustrated in Fig. 9, and as expected, it is similar to the one measured at the ground level—within 3%, as listed in Table II, while considering both neutron kinetic and deposited energies above 10 MeV

In addition to the aforementioned large silicon diode, irradiations at TRIUMF involved a smaller Canberra diode (FD 50-14-300 RM), and several SRAM memories, with a setup example as shown in Fig. 10. As listed in Table III, the detection sensitivity of the large silicon diode exceeds the tested SRAM solutions by five orders of magnitude.

Fig. 11 depicts a detection cross section as calculated for the large diode detector, considering the number of measured events per delivered fluence. As opposed to SRAMs, the cross section for the diode is a function that depends on the limit of the measured deposited energy. The small Canberra diode (with the analogous readout chain) has a significantly lower detection limit (around 200 keV), however, because smaller

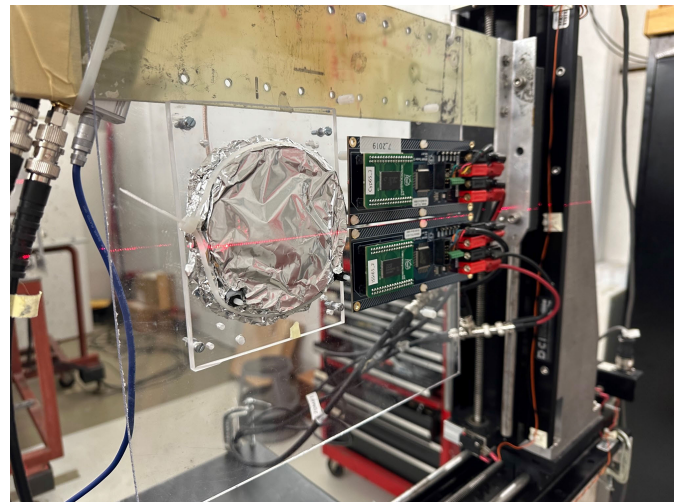


Fig. 10. Silicon detector and two SRAM memories during experimental tests at TRIUMF-BL1B, aiming at demonstrating the enhanced detection capabilities once compared with SRAM solutions.

silicon volume is overall less sensitive at the atmospheric-like neutron detection. At lower threshold energies, the cross section scales with the ratio of silicon volumes. The higher the threshold, the worse the rescaled cross section agreement between the two diodes. This is due to a larger Si range of secondary products, carrying energy outside the sensitive volume.

In addition, as described in Section III-B, the detector can be exploited for dose-rate measurements. An example of measured dose rate during TRIUMF-BL1B irradiation is depicted in Fig. 12. The provided flux of neutrons with kinetic energies  $E_k > 10$  MeV was  $2.2 \cdot 10^5$  n<sub>>10MeV</sub>/cm<sup>2</sup>/s, leading to the deposited dose of  $7 \cdot 10^{-11}$  Gy/(n<sub>>10MeV</sub>/cm<sup>2</sup>) under the exposure to atmospheric-like neutrons. However, due to the limited number of points at Co-60 calibration, this result has a large uncertainty.

### D. Accelerator Environment: LINAC3

To demonstrate the use case for the silicon diode focusing on the accelerator applications, an experiment at one of

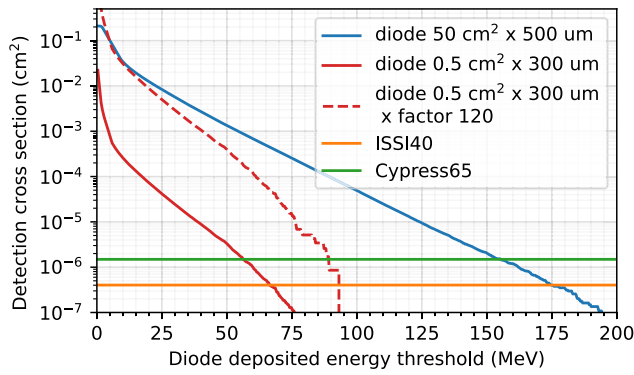


Fig. 11. Detection cross section as a function of the threshold deposited energy, for the large silicon diode, as measured at TRIUMF-BL1B with an atmospheric-like neutron beam. For comparison purposes, the analogous curve for a smaller,  $0.5 \text{ cm}^2 \times 300 \mu\text{m}$ , silicon diode was depicted, together with the measured cross sections for ISSI and Cypress-65 nm memories (listed in Table III). A dashed line corresponds to the detection cross section for a smaller diode rescaled according to the volume ratio ( $\times 120$ ) when compared with the larger detector.

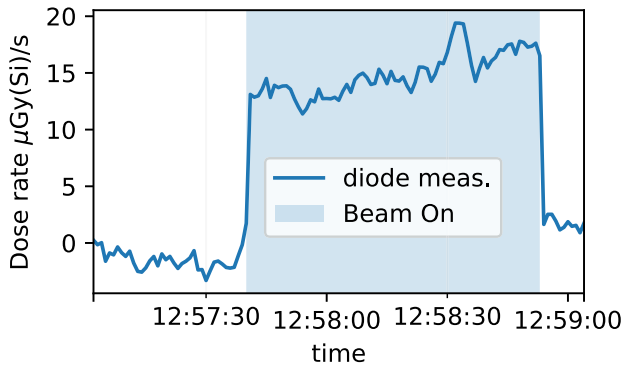


Fig. 12. Measured dose rate during neutron irradiation at BL1B, TRIUMF, with atmospheric-like spectrum. The mean neutron flux ( $> 10 \text{ MeV}$ ) during the run was  $2.2 \cdot 10^5 \text{ n/cm}^2/\text{s}$ .

CERN accelerators, LINAC3, was performed. The aim was to measure the response of multiple radiation detector types under the radiation field that would be produced in case of the sudden loss of  $4.2 \text{ MeV/u}$   $^{16}\text{O}^{8+}$  beam on a magnet or other beamline element. For this reason, different target materials were installed inside the accelerator's vacuum chamber and exposed to the  $^{16}\text{O}^{8+}$  beam. Focusing on the target made of Al, the benchmark between battery-powered RadMon (BatMon) and the silicon diode was performed. The setup is depicted in Fig. 13. The produced radiation field consisted primarily of neutrons, with the simulated spectrum depicted in Fig. 6.

During 4320 s of data acquisition, approximately  $6.6 \cdot 10^{13}$  ions reached the 0.5-mm Al target. The energy of the oxygen ions at the target was  $4.2 \text{ MeV/u}$ . The produced secondary radiation field consisted of neutrons and gamma rays, with the simulated neutron energy spectrum depicted in Fig. 6. The measured energy deposition spectrum is depicted in Fig. 14 and compared with the FLUKA Monte Carlo simulations. The gamma rays do not contribute to the measured energy deposition spectra (below the acquisition threshold). The measured event rate is factor 2.2 lower than the simulated one; however, the energy deposition profiles match well. The difference could be due to approximations used in the simu-

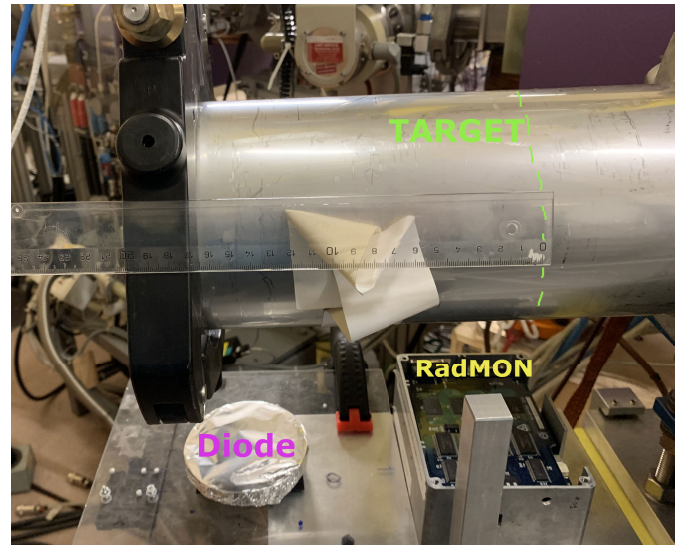


Fig. 13. Silicon diode and BatMon used during LINAC3 experiments aiming in measuring radiation due to loss of a  $4.2\text{-MeV/u}$  oxygen beam on a beamline element. The Al target, mocking a beamline element, was installed inside a vacuum chamber.

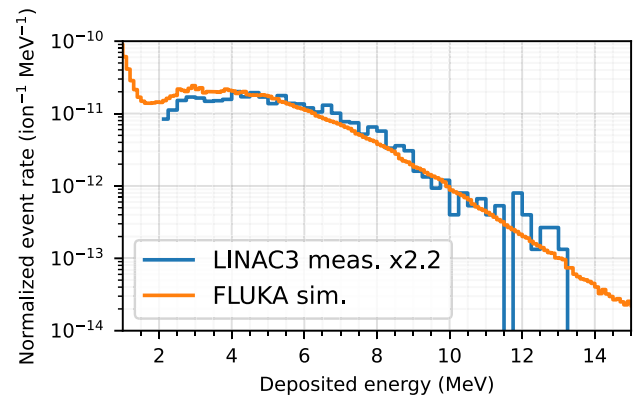


Fig. 14. Measured and simulated energy deposited in the silicon diode as per primary  $^{16}\text{O}^{8+}$  ion impacting the Al target in the LINAC3 at CERN. Measured values were multiplied by 2.2 for visibility purposes.

lations or an overestimated number of ions that reached the target (due to reduced transmission). The measured spectrum below  $\sim 4 \text{ MeV}$  could be affected by the detection limit of the setup. The silicon diode detected 2636 events with the deposited energy above 2 MeV (41 events above 10 MeV deposited). At the same time, BatMon measured 0 SEUs ( $\text{HEHeq} < 5 \cdot 10^6 \text{ cm}^{-2}$ ) and TID below the detection limit of the floating gate transistor ( $< 5 \text{ mGy}$ ) [29]. This demonstrates how the diode detector could efficiently complement RadMON, particularly through the enhancement in detection capabilities. The increased sensitivity could be exploited in CERN's very low radiation areas, where RadMon is not sensitive enough to retrieve meaningful statistics over short time periods. Profiting from the information about an entire energy deposition spectrum, the diode could also be deployed in the regions, where radiation levels are assessed with Monte Carlo simulations, for their validation. Despite the highlighted advantages, the diode detector is significantly more expensive and harder to deploy when compared with the SRAM-based

solutions (such as RadMON), and therefore, the use of diodes in a spatially distributed manner is not foreseen.

## V. CONCLUSION

This article presents a large-volume silicon diode that is considered to be a complementary detector within the low-radiation areas of the CERN accelerator complex, due to its excellent demonstrated detection capabilities, with a sensitivity of five orders of magnitude higher than SRAM-based solutions. The enhanced sensitivity allows for collecting meaningful statistics in significantly reduced time scales. This is relevant, for example, to check the impact of the accelerator parameters on the radiation levels in the shielded alcoves, in view of extrapolating to a high-luminosity LHC upgrade, in which the annual radiation levels (luminosity driven) will increase by a factor of 5.

In addition, the setup is able to measure the deposited energy on an event-by-event basis, allowing to retrieve energy deposition spectrum. We presented the related energy calibration with the monoenergetic proton and alpha beams, and the applications for the detection of low-intensity spectral fields, for example, atmospheric radiation, or Am-Be source.

The agreement between the expected count rate above 10 MeV of deposited energy, as retrieved via simulations for ground level in Geneva (Switzerland), and the actual measurements is within 25%. The atmospheric measurements were compared with the spallation neutrons' measurements collected at TRIUMF-BL1B (Canada), yielding 3% agreement at higher energies (above 10 MeV deposited).

Finally, we presented the use of the detector within the very low-intensity radiation field at the CERN accelerator complex demonstrating its excellent sensitivity.

## ACKNOWLEDGMENT

The authors would like to thank to Pierre Carbonez for support with the Am-Be source.

## REFERENCES

- [1] R. G. Alía et al., "LHC and HL-LHC: Present and future radiation environment in the high-luminosity collision points and RHA implications," *IEEE Trans. Nucl. Sci.*, vol. 65, no. 1, pp. 448–456, Jan. 2018.
- [2] K. Bilko, R. G. Alía, S. Girard, and M. Sebban, "Overview of total ionizing dose levels in the large hadron collider during 2022 restart," in *Proc. IPAC*, Geneva, Switzerland, May 2023, pp. 4008–4011. [Online]. Available: <https://indico.jacow.org/event/41/contributions/2667>
- [3] G. Spiezia et al., "The LHC radiation monitoring system—RadMon," *Proc. Sci.*, vol. 143, pp. 1–12, Oct. 2012.
- [4] G. Spiezia et al., "A new Radmon version for the LHC and its injection lines," *IEEE Trans. Nucl. Sci.*, vol. 61, no. 6, pp. 3424–3431, Dec. 2014.
- [5] A. Ferrari et al., "FLUKA: A multi-particle transport code," CERN, Geneva, Switzerland, CERN Yellow Rep., 10–2005, Jan. 2005.
- [6] T. T. Böhlen et al., "The FLUKA code: Developments and challenges for high energy and medical applications," *Nucl. Data Sheets*, vol. 120, pp. 211–214, Jun. 2014.
- [7] C. Ahdida et al., "New capabilities of the FLUKA multi-purpose code," *Frontiers Phys.*, vol. 9, Jan. 2022, Art. no. 788253. [Online]. Available: <https://www.frontiersin.org/articles/10.3389/fphy.2021.788253/full>
- [8] M. Brugger, "R2E and Availability," in *Proc. LHC Perform. Workshop*, May 2015, pp. 149–160. [Online]. Available: <https://cds.cern.ch/record/2020930>
- [9] Y. Q. Aguiar et al., "Implications and mitigation of radiation effects on the CERN SPS operation during 2021," in *Proc. 13th IPAC*, Geneva, Switzerland, Jul. 2022, pp. 740–743.
- [10] L. Evans and P. Bryant, "LHC machine," *J. Instrum.*, vol. 3, no. 8, Aug. 2008, Art. no. S08001, doi: [10.1088/1748-0221/3/08/S08001](https://doi.org/10.1088/1748-0221/3/08/S08001).
- [11] K. Bilko et al., "Radiation environment in the LHC arc sections during run 2 and future HL-LHC operations," *IEEE Trans. Nucl. Sci.*, vol. 67, no. 7, pp. 1682–1690, Jul. 2020.
- [12] K. Bilko et al., "Silicon solid-state detectors for monitoring high-energy accelerator mixed field radiation environments," in *Proc. 21st Eur. Conf. Radiat. Effects Compon. Syst. (RADECS)*, Sep. 2021, pp. 1–5.
- [13] F. Wrobel et al., "A silicon diode-based detector for investigations of atmospheric radiation," *IEEE Trans. Nucl. Sci.*, vol. 60, no. 5, pp. 3603–3608, Oct. 2013.
- [14] C. Cazzaniga, R. G. Alía, M. Kastriotou, M. Cecchetto, P. Fernandez-Martinez, and C. D. Frost, "Study of the deposited energy spectra in silicon by high-energy neutron and mixed fields," *IEEE Trans. Nucl. Sci.*, vol. 67, no. 1, pp. 175–180, Jan. 2020.
- [15] F. Scholze, H. Henneken, P. Kuschnerus, H. Rabus, M. Richter, and G. Ulm, "Determination of the electron-hole pair creation energy for semiconductors from the spectral responsivity of photodiodes," *Nucl. Instrum. Methods Phys. Res. A, Accel. Spectrom. Detect. Assoc. Equip.*, vol. 439, no. 2, pp. 208–215, Jan. 2000. [Online]. Available: <https://www.sciencedirect.com/science/article/pii/S0168900299009377>
- [16] J. Gómez-Camacho et al., "Research facilities and highlights at the Centro Nacional de Aceleradores (CNA)," *Eur. Phys. J. Plus*, vol. 136, no. 3, p. 273, Mar. 2021.
- [17] Y. Morilla et al., "Progress of CNA to become the Spanish facility for combined irradiation testing in aerospace," in *Proc. 18th Eur. Conf. Radiat. Effects Compon. Syst. (RADECS)*, Sep. 2018, pp. 1–5.
- [18] F. Pozzi et al., "CERN irradiation facilities," *Radiat. Protection Dosimetry*, vol. 180, pp. 120–124, Sep. 2017.
- [19] E. W. Blackmore, "Operation of the TRIUMF (20–500 MeV) proton irradiation facility," in *Proc. IEEE Radiat. Effects Data Workshop. Workshop Rec., Held Conjoint IEEE Nucl. Space Radiat. Effects Conf.*, Jul. 2000, pp. 1–5.
- [20] E. W. Blackmore, "Development of a large area neutron beam for system testing at TRIUMF," in *Proc. IEEE Radiat. Effects Data Workshop*, Jul. 2009, pp. 157–160.
- [21] E. W. Blackmore and M. Trinczek, "Intensity upgrade to the TRIUMF 500 MeV large-area neutron beam," in *Proc. IEEE Radiat. Effects Data Workshop (REDW)*, Jul. 2014, pp. 1–5.
- [22] N. Biancacci et al., "Linac3, LEIR and PS performance with ions in 2021 and prospects for 2022," *JACoW IPAC*, vol. 2022, pp. 1983–1986, Jan. 2022. [Online]. Available: <https://cds.cern.ch/record/2845804>
- [23] M. Cecchetto, R. G. Alía, S. Gerardin, M. Brugger, A. Infantino, and S. Danzeca, "Impact of thermal and intermediate energy neutrons on SRAM SEE rates in the LHC accelerator," *IEEE Trans. Nucl. Sci.*, vol. 65, no. 8, pp. 1800–1806, Aug. 2018.
- [24] TRIUMF. *NIF Beam Specifications*. Accessed: Apr. 26, 2023. [Online]. Available: <https://www.triumf.ca/nif-beam-specifications>
- [25] RadMod Research. *MAIRE*. Accessed: Jan. 12, 2022. [Online]. Available: <https://www.radmod.co.uk/maire>
- [26] M. Cecchetto et al., "0.1–10 MeV neutron soft error rate in accelerator and atmospheric environments," *IEEE Trans. Nucl. Sci.*, vol. 68, no. 5, pp. 873–883, May 2021.
- [27] D. Lucsányi, R. G. Alía, K. Bilko, M. Cecchetto, S. Fiore, and E. Pirovano, "G4SEE: A Geant4-based single event effect simulation toolkit and its validation through monoenergetic neutron measurements," *IEEE Trans. Nucl. Sci.*, vol. 69, no. 3, pp. 273–281, Mar. 2022.
- [28] R. G. Alía et al., "Heavy ion energy deposition and SEE intercomparison within the RADNEXT irradiation facility network," *IEEE Trans. Nucl. Sci.*, vol. 70, no. 8, pp. 1596–1605, Aug. 2023.
- [29] M. Bruccoli et al., "Floating gate dosimeter suitability for accelerator-like environments," *IEEE Trans. Nucl. Sci.*, vol. 64, no. 8, pp. 2054–2060, Aug. 2017.